A six dimensional quantum study for atom–triatom reactions: The $H+H_2O \rightarrow H_2+OH$ reaction

Dong H. Zhang and John C. Light
Department of Chemistry and The James Franck Institute, The University of Chicago, Chicago, Illinois 60637

(Received 15 November 1995; accepted 22 December 1995)

A time-dependent wave packet method has been developed to study atom–triatom ABC+D→AB+CD reactions in full six dimensions (6D). The approach employs a body-fixed coupled angular momentum basis for three angular coordinates, and three 1D bases for three radial coordinates. It permits the calculation of diatom AB vibrational state resolved total reaction probability for an initial rovibrational state of the triatom ABC. The approach is applied to study the $H+H_2O \rightarrow H_2+OH$ reaction on the modified Schatz–Elgersman potential energy surface. Initial state-selected total reaction probabilities are presented for initial ground and several vibrationally excited states of H_2O for total angular momentum $J=0$, along with the final OH vibrational state distributions. We also report the cross sections for reaction from the initial ground vibrational and the first bending excited states of H_2O. Comparisons are made between our results and those from other theoretical calculations and experiments. © *1996 American Institute of Physics.* [S0021-9606(96)01112-4]

I. INTRODUCTION

Significant progress has been made recently in quantum reactive scattering study of four-atom chemical reactions in the gas phase. Starting from the 2D,[1,2] 3D,[3–13] and 4D[14–16] reduced dimensionality quantum calculations for four-atom reactions, it is now possible to carry out quantum calculations for diatom–diatom reactions in full dimension. Benchmark reaction probabilities have been reported for the ''simplest'' reaction $H_2+OH \rightarrow H+H_2O$[17–22] as well as integral cross sections[18,19] and rate constants.[18,19,21] Accurate quantum dynamical studies have also been performed for the isotopically substituted reaction, $HD+OH \rightarrow H+HOD$, $D+H_2O$.[23,24] Very recently, a 5D[25] quantum study has been reported for the $HO+CO \rightarrow H+CO_2$ reaction, a very heavy system with deep wells, which implies that quantum scattering calculations can now be applied to a number of diatom–diatom reactions for total reaction probabilities from some selected initial states.

In contrast to the current status of diatom–diatom reactive scattering calculations, the atom–triatom reaction study is obviously less developed. So far, a state-to-state reaction probability study has been reported only for the $H+H_2O \leftrightarrow H_2+OH$ reaction in planar configuration (4D).[14] Most theoretical investigations on atom-triatom reactions are done by either quasiclassical trajectory calculations,[26–30] or 3D reduced dimensionality quantum studies.[3,4,6,8–12,31] While these methods address many interesting and important properties of these reactions, there remain uncertainties in the results given by these methods. Thus an exact quantum method for 6D atom–triatom reactions is of substantial interest.

In this paper, we develop a time-dependent wave packet method to treat the atom–triatom ABC+D→AB+CD reaction in full dimension, which is capable of calculating the final diatom AB vibrational state resolved total reaction probabilities for an initial rovibrational state of the triatom ABC. By employing a body-fixed (BF) coupled total angular momentum basis for three angle coordinates, and three 1D bases for the three radial coordinates in the 6D wave function expansion, we can very easily and efficiently take the advantage of time-dependent approach to reactive scattering, and make it possible to carry out some atom–triatom reactive scattering calculations in 6D in a medium size workstation. This choice of wave function expansion also makes the present approach similar in many aspects to the time-dependent wave packet approach to diatom–diatom reactions,[17–19,23–25] enabling us to utilize several techniques developed in diatom–diatom reaction studies. The theory is applied to the ''simplest'' atom–triatom reaction, the $H+H_2O \rightarrow H_2+OH$ on the Schatz–Elgersma (WDSE) potential energy surface[32–34] slightly modified by Clary.[3] We report in this paper detailed initial state-selected reaction probabilities from several initial vibrational states of H_2O, with the final vibrational states of OH resolved. We also report the cross sections, for reaction from ground vibrational and the first bending excited state of H_2O. Although the calculations include all six dimensions, we do not impose the full quantum permutation symmetry on the H atoms, and one OH bond in H_2O is restricted to bound vibrational states due to the restriction from both the WDSE PES and the computational effort required.

The $H+H_2O$ and its isotopically substituted analogs comprise one of the simplest polyatomic reaction systems in which there are several different vibrational modes of a polyatomic reactant. Extensive experiments have been carried out to measure the thermal rate constants,[35–38] to study the influence of translational energy and isotopic substitution on the absolute reaction cross section and the final state distribution,[39–44] and to study the influence of initial vibrational excitation of H_2O and its isotopically substituted counterparts on the reaction dynamics.[45–53] Theoretically, since

 0021-9606/96/104(12)/4544/10/$10.00

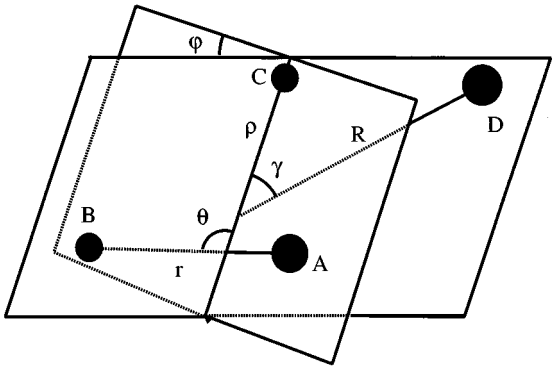

FIG. 1. The Jacobi coordinates for the atom–triatom system.

the first pioneering quasiclassical trajectory studies of Schatz *et al.* in 1984,[26,27] there have been a number of other studies, quasiclassical[28–30] and reduced dimensionality quantum mechanical,[3,4,6,8–12,31] devoted to understanding the dynamics in these reactions.

This paper is organized as follows: In Sec. II, we present the time-dependent method for atom–triatom reactions in full six dimensions. In Sec. III, detailed numerical aspects, total reaction probabilities, and integral cross sections for several initial vibrational states for the H+H_2O→H_2+OH reaction are reported with the comparisons with other theoretical results and with experimental measurements. Section IV gives a summary of our results and conclusions.

II. THEORY

A. 6D Atom–triatom Hamiltonian

The 6D Hamiltonian for an atom–triatom system expressed in the Jacobi coordinates shown in Fig. 1 can be written as

$$H=-\frac{\hbar^2}{2\mu}\frac{\partial^2}{\partial R^2}+\frac{(\mathbf{J}-\mathbf{L})^2}{2\mu R^2}+h_r(r)+h_\rho(\rho)+\frac{\mathbf{j}^2}{2\mu_r r^2}+\frac{\mathbf{l}^2}{2\mu_\rho \rho^2}+V(R,r,\rho,\theta,\gamma,\phi), \tag{1}$$

where μ_r is the reduced mass of diatom AB, μ_ρ is the reduced mass of diatom AB and atom C, μ is the reduced mass of the triatom ABC and atom D, r is the bond length of diatom AB, ρ is the distance from the center of mass of diatom AB to atom C, R is the distance from the center of mass of triatom ABC to atom D, **J** is the total angular momentum operator, **j** is the rotational angular momentum operator for diatom AB, **l** is orbital momentum operator of C with respect to diatom AB; **j** and **l** are coupled to form the total angular momentum **L** of triatom ABC.

The 1D reference Hamiltonians $h_r(r)$ and $h_\rho(\rho)$ in Eq. (1) are defined as

$$h_r(r)=-\frac{\hbar^2}{2\mu_r}\frac{\partial^2}{\partial r^2}+v_r(r), \tag{2}$$

$$h_\rho(\rho)=-\frac{\hbar^2}{2\mu_\rho}\frac{\partial^2}{\partial \rho^2}+v_\rho(\rho), \tag{3}$$

where $v_r(r)$ and $v_\rho(\rho)$ are the 1D reference potentials for r and ρ obtained from the total interaction potential $\mathbf{V}(R,r,\rho,\theta,\gamma,\phi)$ with other degrees of freedom fixed at specific values as follows:

$$v_r(r)=\mathbf{V}(R\to\infty,r,\rho=\rho_0,\theta=\theta_0,\gamma,\phi), \tag{4}$$

$$v_\rho(\rho)=\mathbf{V}(R\to\infty,r=r_0,\rho,\theta=\theta_0,\gamma,\phi), \tag{5}$$

with r_0, ρ_0 and θ_0 fixed at the equilibrium Jacobi coordinates for the triatomic ABC molecule far away from atom D. The interaction potential $V(R,r,\rho,\theta,\gamma,\phi)$ in Eq. (1) is thus equal to:

$$V(R,r,\rho,\theta,\gamma,\phi)=\mathbf{V}(R,r,\rho,\theta,\gamma,\phi)-v_r(r)-v_\rho(\rho). \tag{6}$$

B. Rotational basis for atom–triatom system

In order to make it easy to understand the total angular momentum rotational basis for atom–triatom system, it will be helpful to define three reference frames, namely a space-fixed (SF) frame, a body-fixed (BF) frame, and a molecular fixed (MF) frame. The BF frame, rotating with the atom-triatom complex, is defined such that the BF z axis lies along the vector **R**, which points from the center of mass of the triatom to the atom. The z axis of the MF frame lies along the vector $\boldsymbol{\rho}$ pointing from the center of mass of diatom AB to the atom C. Here, one can note that the BF and MF frames for atom–triatom system are equivalent, respectively, to the spaced-fixed and body-fixed frames for diatom AB and atom C system which have been thoroughly understood in atom-diatom studies.[54] The overall rotational basis function for an atom–triatom system in the BF frame then can be written as

$$\mathbf{Y}^{JM}_{jlL\Omega}(\hat{r},\hat{\rho},\hat{R})=Y^{L\Omega}_{jl}(\hat{r},\hat{\rho})N^J_{M,\Omega}(\hat{R}), \tag{7}$$

where

$$N^J_{M,\Omega}(\hat{R})=\sqrt{\frac{2J+1}{4\pi}}D^{J*}_{M\Omega}(\alpha,\beta,0) \tag{8}$$

are eigenfunctions of $\mathbf{J}^2$ and depend on the angles which rotate the SF axes on to the BF axes.

$$Y^{L\Omega}_{jl}(\hat{r},\hat{\rho})=\sum_K D^{L*}_{\Omega K}(\chi,\gamma,\phi)\sqrt{\frac{2l+1}{4\pi}}\langle jKl0|LK\rangle y_{jK}(\theta,0), \tag{9}$$

is the rotational basis for diatom AB and atom C where L and Ω are, respectively, the total angular momentum and its projection on the BF z axis of atom–triatom system for triatom ABC.[54] In Eq. (9), $y_{jK}(\theta,0)$ is a spherical harmonic, $\langle jKl0|LK\rangle$ is a Clebsch–Gordan coefficient. The function $D^{J*}_{M\Omega}(\alpha,\beta,0)$ in Eq. (8) and $D^{L*}_{\Omega K}(\chi,\gamma,\phi)$ in Eq. (9) are the elements of the Wigner rotation matrix.

In order to examine the parity we use the space fixed frame. The rotational basis function $\mathbf{Y}^{JM}_{jlL\Omega}(\hat{r},\hat{\rho},\hat{R})$ can be written in terms of the unitary transformation of the basis function $X^{JM\epsilon}_{jlLN}(\hat{r}'\hat{\rho}'\hat{R})$ from a space-fixed frame as,[54–56]

$$\mathbf{Y}^{JM}_{jlL\Omega}(\hat{r},\hat{\rho},\hat{R})=\sum_N \left(\frac{2N+1}{2J+1}\right)^{1/2}\langle L\Omega N0|J\Omega\rangle X^{JM\epsilon}_{jlLN}(\hat{r}'\hat{\rho}'\hat{R}), \tag{10}$$

where $X^{JM\epsilon}_{jlLN}(\hat{r}'\hat{\rho}'\hat{R})$ can be written in the usual way as:

$$\begin{aligned}X^{JM\epsilon}_{jlLN}(\hat{r}'\hat{\rho}'\hat{R})=&\sum_{m_j m_l m_L m_N}\langle Lm_L Nm_N|JM\rangle\\&\times\langle jm_j lm_l|Lm_L\rangle\\&\times y_{jm_j}(\hat{r}')y_{lm_l}(\hat{\rho}')y_{Nm_N}(\hat{R})\end{aligned} \tag{11}$$

with N the orbital angular momentum for atom D with respect to molecule ABC. The effect of the parity operator, $\hat{\epsilon}$, is to invert the space-fixed coordinates in the origin: $(\hat{r}',\hat{\rho}',\hat{R})\rightarrow(-\hat{r}',-\hat{\rho}',-\hat{R})$. Applying $\hat{\epsilon}$ to Eq. (11), we can easily get

$$\begin{aligned}\hat{\epsilon}X^{JM\epsilon}_{jlLN}(\hat{r}'\hat{\rho}'\hat{R})&=X^{JM\epsilon}_{jlLN}(-\hat{r}'-\hat{\rho}'-\hat{R})\\&=(-1)^{j+l+N}X^{JM\epsilon}_{jlLN}(\hat{r}'\hat{\rho}'\hat{R}).\end{aligned} \tag{12}$$

So in the SF frame, the parity $\epsilon=(-1)^{j+l+N}$.

Now applying $\hat{\epsilon}$ to Eq. (10), we get:

$$\begin{aligned}\hat{\epsilon}\mathbf{Y}^{JM}_{jlL\Omega}(\hat{r},\hat{\rho},\hat{R})&=\sum_N\left(\frac{2N+1}{2J+1}\right)^{1/2}\langle L\Omega N0|J\Omega\rangle\\&\times(-1)^{j+l+N}X^{JM\epsilon}_{jlLN}(\hat{r}'\hat{\rho}'\hat{R})\\&=\sum_N\left(\frac{2N+1}{2J+1}\right)^{1/2}(-1)^{L+N+J}\\&\times\langle L-\Omega N0|J-\Omega\rangle\\&\times(-1)^{j+l+N}X^{JM\epsilon}_{jlLN}(\hat{r}'\hat{\rho}'\hat{R})\\&=(-1)^{J+j+l+L}\mathbf{Y}^{JM}_{jlL-\Omega}(\hat{r},\hat{\rho},\hat{R}).\end{aligned} \tag{13}$$

Thus we find the rotation basis functions in Eq. (7) are not eigenfunctions of the parity operator since $\Omega\rightarrow-\Omega$. Functions with well defined parity, ϵ, are constructed by taking linear combinations of Eq. (7):

$$\begin{aligned}\mathbf{Y}^{JM\epsilon}_{jlL\bar{\Omega}}(\hat{r},\hat{\rho},\hat{R})=&[2(1+\delta_{\bar{\Omega}0})]^{-1/2}[\mathbf{Y}^{JM}_{jlL\bar{\Omega}}(\hat{r},\hat{\rho},\hat{R})\\&+\epsilon(-1)^{J+l+j+L}\mathbf{Y}^{JM}_{jlL-\bar{\Omega}}(\hat{r},\hat{\rho},\hat{R})],\end{aligned} \tag{14}$$

where $\bar{\Omega}=|\Omega|$. The $(\mathbf{J}-\mathbf{L})^2$ matrix elements in the BF representation are given by

$$\begin{aligned}&\langle\mathbf{Y}^{JM\epsilon}_{jlL\bar{\Omega}}|(\mathbf{J}-\mathbf{L})^2|\mathbf{Y}^{JM\epsilon}_{jlL\bar{\Omega}'}\rangle\\&=[J(J+1)+L(L+1)-2\bar{\Omega}^2]\delta_{\bar{\Omega}\bar{\Omega}'}\\&\quad-(1+\delta_{\bar{\Omega}0})^{1/2}\lambda^{+}_{J\bar{\Omega}}\lambda^{+}_{L\bar{\Omega}}\delta_{\bar{\Omega}+1\bar{\Omega}'}\\&\quad-(1+\delta_{\bar{\Omega}1})^{1/2}\lambda^{-}_{J\bar{\Omega}}\lambda^{-}_{L\bar{\Omega}}\delta_{\bar{\Omega}-1\bar{\Omega}'},\end{aligned} \tag{15}$$

where the quantity λ is defined as

$$\lambda^{\pm}_{AB}=[A(A+1)-B(B\pm1)]^{1/2}. \tag{16}$$

C. Wavefunction expansion and initial state construction

The time-dependent wavefunction is expanded in terms of the BF (body-fixed) rotation basis functions defined in the previous subsection as:

$$\begin{aligned}\Psi^{JM\epsilon}_{\nu_0L_0\bar{\Omega}_0}(\mathbf{R},\mathbf{r},\boldsymbol{\rho},t)=&\sum_{n,v_1,v_2,j,l,L,\bar{\Omega}}F^{JM\epsilon}_{nv_1v_2jlL\bar{\Omega}}(t)u^{v_2}_n(R)\\&\times\varphi_{v_1}(r)\varphi_{v_2}(\rho)\mathbf{Y}^{JM\epsilon}_{jlL\bar{\Omega}}(\hat{R},\hat{r},\hat{\rho}),\end{aligned} \tag{17}$$

where n is a translational basis label, (ν_0,L_0) denotes the initial rovibrational state of the triatom ABC.

The vibrational bases $\varphi_{v_1}(r)$ and $\varphi_{v_2}(\rho)$ used in Eq. (17) are the the eigenstates of the 1D Hamiltonians h_r and h_ρ, respectively. The translational basis function is defined as,[19]

$$u^{v_2}_n(R)=\begin{cases}\sqrt{\dfrac{2}{R_4-R_1}}\sin\dfrac{n\pi(R-R_1)}{R_4-R_1} & v_2\leqslant v_{\text{asy}}\\ \sqrt{\dfrac{2}{R_2-R_1}}\sin\dfrac{n\pi(R-R_1)}{R_2-R_1} & v_2>v_{\text{asy}},\end{cases} \tag{18}$$

where R_2 and R_4 define, respectively, the interaction and asymptotic grid ranges,[19] and v_{asy} is chosen to define the basis which can accurately expand the first several 3D rovibrational states of molecule ABC far away from Atom D. The definition of $u^{v_2}_n(R)$ in Eq. (18) makes it extremely simple to separate the asymptotic region from the interaction region, and very efficient in achieving computational savings by reducing the vibrational basis for the ρ coordinate where possible.[19]

The initial wave function is chosen as the direct product of a localized translational wave packet for R and a specific $(JM\epsilon)$ state for the atom–triatom system with a specific rovibrational eigenstate $(\nu_0L_0\bar{\Omega}_0)$ for triatom ABC,

$$\Psi^{JM\epsilon}_{\nu_0L_0\bar{\Omega}_0}(\mathbf{R},\mathbf{r},\boldsymbol{\rho},t=0)=G(R)\psi^{JM\epsilon}_{\nu_0L_0\bar{\Omega}_0}(\hat{R},\mathbf{r},\boldsymbol{\rho}), \tag{19}$$

where the wave packet $G(R)$ is chosen to be a standard Gaussian function,

$$G(R)=(\pi\delta^2)^{-1/4}\exp(-(R-R_0)^2/2\delta^2)e^{-ik_0R}. \tag{20}$$

$\psi^{JM\epsilon}_{\nu_0L_0\bar{\Omega}_0}(\hat{R},\mathbf{r},\boldsymbol{\rho})$ is the eigenfunction of the triatom ABC Hamiltonian,

$$\begin{aligned}H_{ABC}=&h_r(r)+h_\rho(\rho)+\frac{\mathbf{j}^2}{2\mu_r r^2}+\frac{\mathbf{l}^2}{2\mu_\rho\rho^2}\\&+V(R\rightarrow\infty,r,\rho,\theta,\gamma,\phi),\end{aligned} \tag{21}$$

with ν_0, L_0, $\bar{\Omega}_0$ representing, respectively, the triatom ABC's initial vibrational state, total angular momentum, and the projection of total angular momentum on the BF z axis of atom–triatom system. The wave function is expanded as,

$$\psi^{JM\epsilon}_{v_0 L_0 \bar{\Omega}_0}(\hat{\mathbf{R}},\mathbf{r},\boldsymbol{\rho}) = \sum_{v_1 v_2 jl}^{v_2 \leqslant v_{\rm asy}} C_{v_1 v_2 jl}\, \varphi_{v_1}(r)\varphi_{v_2}(\rho)\mathbf{Y}^{JM\epsilon}_{jlL_0\bar{\Omega}_0}(\hat{R},\hat{r},\hat{\rho}). \quad (22)$$

When R is sufficiently large, the interaction potential $V(R,r,\rho,\theta,\gamma,\phi)$ in Eq. (21) only depends on r,ρ and θ, i.e., $V(R,r,\rho,\theta,\gamma,\phi) \underset{R\to\infty}{\to} V(r,\rho,\theta)$. Then the potential matrix element on basis $\mathbf{Y}^{JM\epsilon}_{jlL_0\bar{\Omega}_0}$ for fixed r and ρ can easily be evaluated as,

$$\langle \mathbf{Y}^{JM\epsilon}_{jlL_0\bar{\Omega}_0}|V(r,\rho,\theta)|\mathbf{Y}^{JM\epsilon}_{j'l'L_0\bar{\Omega}_0}\rangle = \sum_K \frac{2\pi\sqrt{(2l+1)(2l'+1)}}{2L_0+1}\langle jKl0|L_0K\rangle\langle j'Kl'0|L_0K\rangle \times \langle y_{jK}(\theta,0)|V(r,\rho,\theta)|y_{j'K}(\theta,0)\rangle, \quad (23)$$

exactly the same as for the atom–diatom case.

D. Wave packet propagation and reactive flux calculation

The method used to propagate the initial wave packet and calculate the total reaction probability is essentially the same as that used in the diatom–diatom reactive scattering calculations.[17–19,23–25] Since very detailed descriptions have been given in those references, here we only briefly outline the method for completeness. The split-operator propagator[57] is employed to carry out the wave-packet propagation,

$$\Psi^{JM\epsilon}(\mathbf{R},\mathbf{r},\boldsymbol{\rho},t+\Delta) = e^{-iH_0\Delta/2}e^{-iU\Delta}e^{-iH_0\Delta/2}\Psi^{JM\epsilon}(\mathbf{R},\mathbf{r},\boldsymbol{\rho},t), \quad (24)$$

where the reference Hamiltonian H_0 is defined as,

$$H_0 = -\frac{\hbar^2}{2\mu}\frac{\partial^2}{\partial R^2} + h_r(r) + h_\rho(\rho), \quad (25)$$

and the effective potential operator U in Eq. (24) is defined as

$$U = \frac{(\mathbf{J}-\mathbf{L})^2}{2\mu R^2} + \frac{\mathbf{j}^2}{2\mu_r r^2} + \frac{\mathbf{l}^2}{2\mu_\rho \rho^2} + V(\mathbf{r},\boldsymbol{\rho},\mathbf{R}) = V_{\rm rot} + V(\mathbf{r},\boldsymbol{\rho},\mathbf{R}). \quad (26)$$

As in Refs. 24 and 25, the operation of the interaction potential $V(\mathbf{r},\boldsymbol{\rho},\mathbf{R})$ is treated by quadrature of (θ,γ,ϕ) at a given DVR point (R_k,r_m,ρ_n) because the size of the angular momentum basis $\mathbf{Y}^{JM\epsilon}_{jlL\bar{\Omega}}$ is so large that it is impractical to construct and diagonalize the potential matrix V in that angular momentum basis. We do the quadrature by defining a transformation matrix $\mathbf{Q}$ as

$$Q^{jlL\bar{\Omega}}_{kmn} = \sqrt{\mathbf{W}^\theta_k\mathbf{W}^\gamma_m\mathbf{W}^\phi_n}\langle\theta_k\gamma_m\phi_n|\mathbf{Y}^{JM\epsilon}_{jlL\bar{\Omega}}\rangle, \quad (27)$$

where $(\theta_k\gamma_m\phi_n)$ are angular quadrature points and $(\mathbf{W}^\theta_k,\mathbf{W}^\gamma_m,\mathbf{W}^\phi_n)$ are the quadrature weights for the corresponding angles. Then $e^{-iU\Delta}$ can be approximated by the angular quadrature as,

$$e^{-iU\Delta} = e^{-iV_{\rm rot}\Delta/2}\mathbf{Q}^+e^{-iV\Delta}\mathbf{Q}e^{-iV_{\rm rot}\Delta/2}, \quad (28)$$

where $\mathbf{Q}^+$ is the Hermitian conjugate of $\mathbf{Q}$. In practice, one does not have to store the large matrix $\mathbf{Q}$ but only the few small submatrices necessary to construct Q.

The absorption of the time-dependent wave function at the boundaries during propagation is the same as in Ref. 19, and will not be repeated here.

By the propagation of an initial wave packet $|\Psi_i(0)\rangle$, the total reaction probabilities for that specific initial state for a whole range of energies can be obtained by evaluating the reactive flux at a dividing surface $\rho=\rho_s$ as,[19]

$$P^R_i(E) = \frac{\hbar}{m_1}\,{\rm Im}[\langle\psi^+_{iE}|\psi^{+\prime}_{iE}\rangle]|_{\rho=\rho_s}, \quad (29)$$

where ψ^+_{iE} and $\psi^{+\prime}_{iE}$ are the time-independent (TI) wavefunction ψ^+_{iE} and its normal derivative. ψ^+_{iE} is obtained by performing a Fourier transform of the time-dependent wave function as,[19]

$$|\psi^+_{iE}\rangle = \frac{1}{a_i(E)}\int_{-\infty}^{\infty} e^{(i/\hbar)(E-H)t}|\Psi_i(0)\rangle dt, \quad (30)$$

and similarly for $\psi^{+\prime}_{iE}$. The coefficient $a_i(E)$ is the overlap between the initial wave packet and the energy-normalized asymptotic scattering function, $a_i(E)=\langle\phi_{iE}|\Psi_i(0)\rangle$.[19]

In order to resolve the final vibrational state for diatom AB, ρ_s should be chosen sufficiently large, and the TI wave function ψ^+_{iE} and its derivative are expanded on the asymptotic diatom AB rovibrational basis which are the eigenfunctions of the 1D diatomic Hamiltonian,

$$h^{\rho\to\infty}_r(r) = -\frac{\hbar^2}{2\mu_r}\frac{\partial^2}{\partial r^2} + \mathbf{V}(R\to\infty,r,\rho\to\infty,\theta,\gamma,\phi) + \frac{\mathbf{j}^2}{2\mu_r r^2}. \quad (31)$$

III. RESULTS OF CALCULATIONS

A. Numerical aspects and H_2O vibrational states on the WDSE PES

The 6D time-dependent method is applied to the reaction

$$H+H_2O(\nu_1\nu_2\nu_3,L_0,\bar{\Omega}_0)\to H_2+OH(\nu), \quad (32)$$

where ν_1, ν_2, and ν_3 refer to the symmetric stretching, bending, and asymmetric stretching vibrations of H_2O. Fig. 2 summarizes the energetic considerations for the reaction on the WDSE PES[32–34] which is characterized by a 0.923 eV classical barrier to reaction and an overall endoergicity of 0.659 eV. The PES is also characterized by a relatively low barrier (0.406 eV) to hydrogen exchange (i.e. $H'+H_2O\to H'OH+H$) which is known to be incorrect in both topology and height.[58] Thus we ignore the exchange dynamics here although we do obtain the probabilities for exchange in our calculations. On the WDSE surface, the hydrogen atom can only react with one of the two hydrogen atoms in H_2O, and the collisions with the other hydrogen can only lead to nonreactive scattering.[58] Thus we treat one OH bond as a

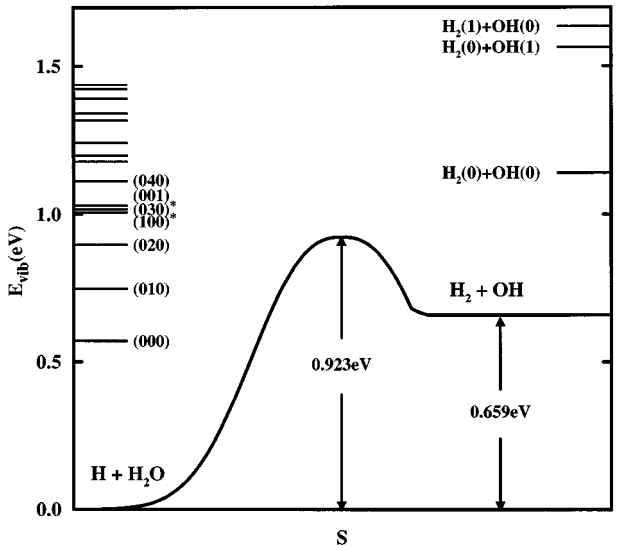

FIG. 2. Potential energy along reaction path for the H+H_2O→H_2+OH reaction with some vibrational state energies for reactant and product.

nonreactive bond in our calculations, and multiply the *cross sections* by a factor of 2 to compare with other theoretical and experimental results, based on the fact that the hydrogen atom can react equally with either hydrogen in H_2O. [Our method, in principle, is capable of allowing either of the two OH bonds to be broken in reaction by using a sufficiently large vibrational basis for the r coordinate in Eq. (17).]

All the results presented in this paper are for the H_2O molecule in an initial nonrotating state, i.e. $L_0=0$, and for the even parity of the system. The reaction probabilities are for total angular momentum $J=0$, and cross sections are calculated by using the centrifugal sudden (CS) approximation.[59,60] The interaction region is defined by a rectangular box of $[1.2, 5.0]a_0$ in ρ and $[1.4, 5.2]a_0$ in the R coordinate. A total of 25 vibrational basis functions, $\varphi_{v_2}(\rho)$, and 30 sine DVR points on the R coordinate are used in the wave function expansion in the interaction region. The asymptotic region is defined from 5.2 to 9.4 a_0 in R, in which we used 7 vibrational basis functions and 32 sine DVR points. The number of vibrational basis functions $\varphi_{v_1}(r)$ for the non-reactive OH is 3 for both interaction and asymptotic regions. The rotational basis is large. We used $j_{\max}=13$, and $l_{\max}=30$, resulting $L_{\max}=43$ in our calculations. The number of rotational basis functions is 2800 for the case of even parity. Thus the total basis is over 8 million functions. The initial wave packet is centered at $R=7.0$ a_0 with a narrow width of 0.4 a_0. We propagated the wave packet for a total time of 3000 a.u., with a time step of 15 a.u., to obtained well converged reaction probabilities.

Table I gives the first several vibrational state energies, their spectroscopic assignments, and corresponding root-mean-square deviations of the bending angle, $\Delta\theta$, for nonrotating H_2O molecule on the WDSE PES. It should be pointed out that the 4th and 5th vibrational states are actually in strong Fermi resonance. The 4th state has a slightly larger component of (100) state than the 5th state, thus we assigned the 4th & 5th states as (100)* & (030)*, respectively, with the * to indicate that the assignments are not rigorous.

TABLE I. The first seven vibrational energy levels of nonrotating H_2O on the WDSE PES. The energies are relative to the ground state energy of 0.571 eV. $\Delta\theta$ is in degree.

n	Energy (eV)	$\Delta\theta$	$(\nu_1\nu_2\nu_3)$
1	0.00	9.09	(000)
2	0.177	16.27	(010)
3	0.328	22.45	(020)
4	0.437	22.38	(100)*
5	0.448	26.54	(030)*
6	0.458	9.20	(001)
7	0.546	30.92	(040)

B. Total reaction probabilities

The total reaction probabilities as a function of total energy are shown in Figs. 3 and 4 for H_2O initially in the ground vibration state (000), the bending excited states (010), (020), (030)*, and (040), the symmetric stretch excited state (100)*, and the asymmetric stretch excited (001). The total energy is measured with respect to the energy of nonrotating H_2O(000), so for the (000) state it is equal to the asymptotic translational energy. Figure 3 shows the reaction probabilities for the low energy region up to 1.1 eV, and Fig. 4 gives those for energy up to 1.8 eV. In Fig. 5, we show the total reaction probabilities as a function of translational energy for all these initial states.

For the (000) state, the reaction probability increases steadily with increasing translational energy starting from about 0.73 eV. We found in our dynamics calculations that the collision of the H atom with the reactive hydrogen atom in H_2O will most likely lead to hydrogen *exchange* reaction. Only a small fraction of the wave function with small γ

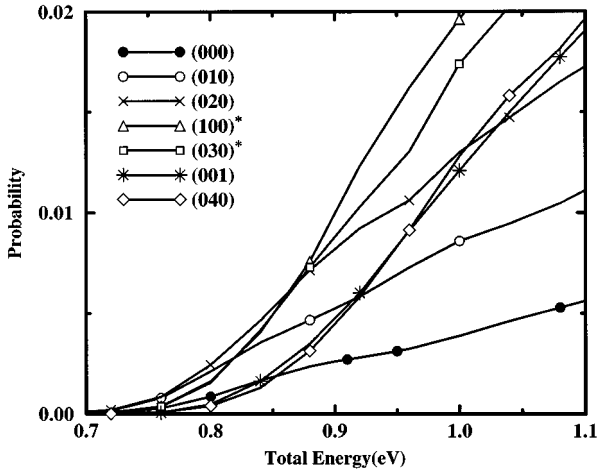

FIG. 3. Initial state selected total reaction probabilities for the reaction H+$H_2O(\nu_1\nu_2\nu_3)$→H_2+OH for total angular momentum $J=0$ as a function of total energy to 1.1eV, measured with respect to the energy of H_2O ground rovibrational state. The initial vibrational states of H_2O are (000) (solid circles), (010) (open circles), (020) (crosses), (100)* (triangles), (030)* (squares), (001) (stars), and (040) (diamonds).

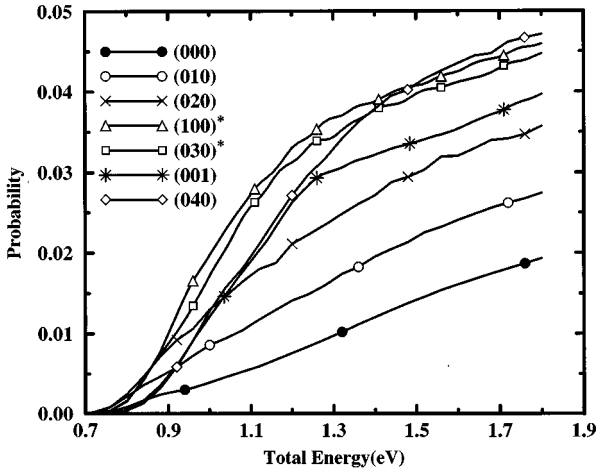

FIG. 4. Similar to Fig. 3 except the total energy up to 1.8 eV.

contributes to the hydrogen extraction reaction, so the overall reaction probability is very small ($P_{\text{react}}=0.019$ for $E_{\text{trans}}=1.8$ eV). This was also found in the QCT[27] and quantum 4D planar[14] calculations.

In general, different initial vibrational excitations of H_2O substantially enhance reactivity as can be seen very clearly from Fig. 5. For the first four vibrationally excited initial states, as shown in Fig. 4 the reactivity at fixed total energy increases with increasing internal excitation energy, and the threshold energies for these states are even a little lower than that for the (000) state. These are measured in *total energy*, which means that all the vibration energy deposited in H_2O is used to reduce the threshold. For the initial (001) and (040) states, however, the total reaction probabilities for low total energies are smaller than for the ground (000) state as shown in Fig. 3. But for total energy larger than 0.9 eV the reactivities from these two initial states are very clearly enhanced. For high total energy the initial (040) state even gives the largest in reactivity among all the initial states. Thus the extremely high efficiency of threshold reduction of the first four vibrationally excited states begins to drop slightly in the fifth state, i.e. (001) state, and the sixth state, i.e. (040) state. The asymmetric stretch excited state (001), which is 0.021 eV and 0.01 eV higher in vibration excitation energy than the (100)* and (030)* states, respectively, gives substantially smaller reaction probability, indicating the asymmetric stretching excitation is less efficient in enhancing reactivity than the symmetric stretching excitation.

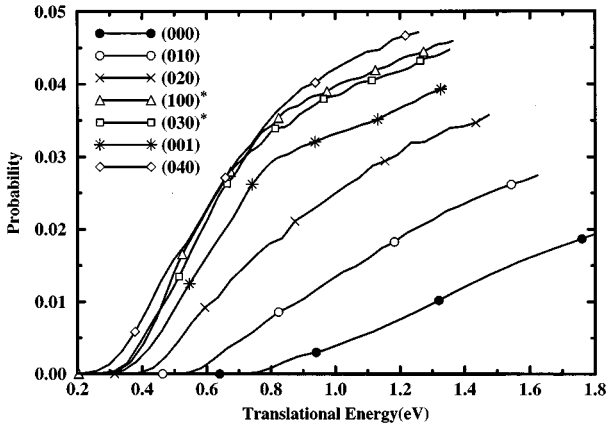

FIG. 5. Similar to Fig. 4 except that the reaction probabilities are plotted as a function of translational energy.

The trend in the threshold reduction here is essentially the same as that found earlier in quantum 4D planar calculations,[14] although there exist substantial quantitative differences between these two calculations. The 4D planar calculation[14] gives threshold energies almost 0.1 eV lower than the present calculation; and the rise in reaction probability from threshold also is much steeper than the present results for all states. QCT calculations[27] found that the cross section thresholds drop by about 96% of the excitation energies for the first two bending states, and the threshold for the (030) state is about the same as for (020) state measured in translational energy. This indicates that the high efficiency of threshold reduction from the first two bending excitations does not persist for higher overtones. QCT calculations[27] also showed that the symmetric stretching excitation is more efficient in enhancing the reactivity than the asymmetric stretching excitation. Although the behavior of the reaction probability is not necessarily the same as that of the cross section, we still can say that the qualitative agreement between the present and QCT[27] calculations is reasonably good.

C. Product OH vibration distribution

The present calculations find that the probabilities to form product OH in the first excited vibration state (P[OH(1)]) are very small except for the initial excitation of the (001) state. For the (000), (010), (020), and (040) states, P[OH(0)] are so close to the total reaction probabilities for all the energies that these two curves will just overlap if we plotted them together. Thus we only show P[OH(0)] and P[OH(1)] together with the total reaction probabilities for (100)*, (030)* and (001) states in Fig. 6. Only for energy higher than 1.2 eV we can see some significant amount of OH(1) product, while the threshold energy to produce OH(1) in final product is 0.993 eV as can be seen from Fig. 2.

The product ratio, OH(1)/OH(0), for all states as a function of total energy is shown in Fig. 7. Due to the extremely small probabilities in the low energy region, these values can only be regarded as the upper limit for the ratio for the energy between 1.0 to 1.2 eV. As can be seen from the figure, the excitation ratio for the initial $H_2O(000)$ state is very small; for E=1.8 eV, it is only 0.9%. This small ratio is in agreement with several experimental observations,[39,42,52] in particular the recent experiment of Jacobs *et al.* who determined the upper limit for the cross section OH(1)/OH(0) ratio to be 0.01 for all collision energy up to 2.7 eV.[42] From the fact that the first two and the fourth bending excitations have only tiny effect on the ratio, we deduce that the *pure* initial bending excitation has essentially no effect on the ra-

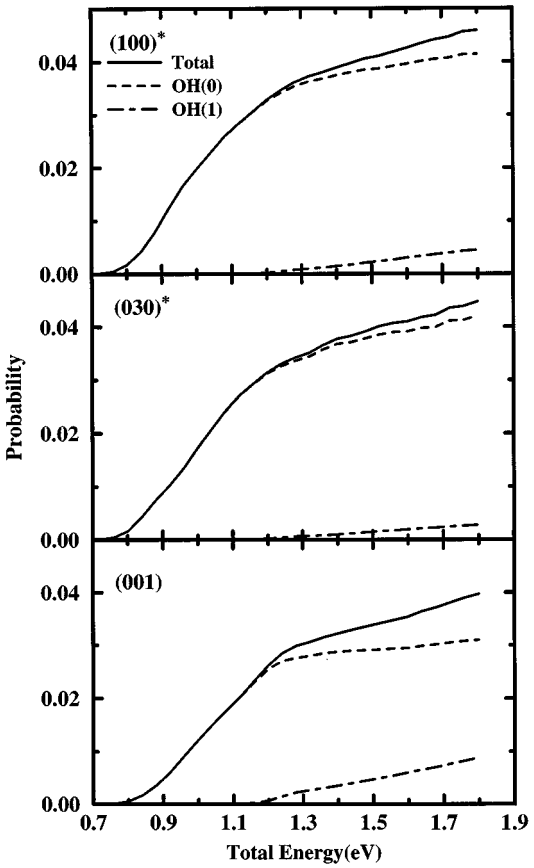

FIG. 6. Product OH vibration distributions for the the $H+H_2O(\nu_1\nu_2\nu_3) \rightarrow H_2+OH(\nu)$ reaction for H_2O initially in (100)*, (030)* and (001) states as a function of total energy. The dashed lines are for product OH(0), the dot-dashed lines for product OH(1), and the solid lines for the total reaction probabilities.

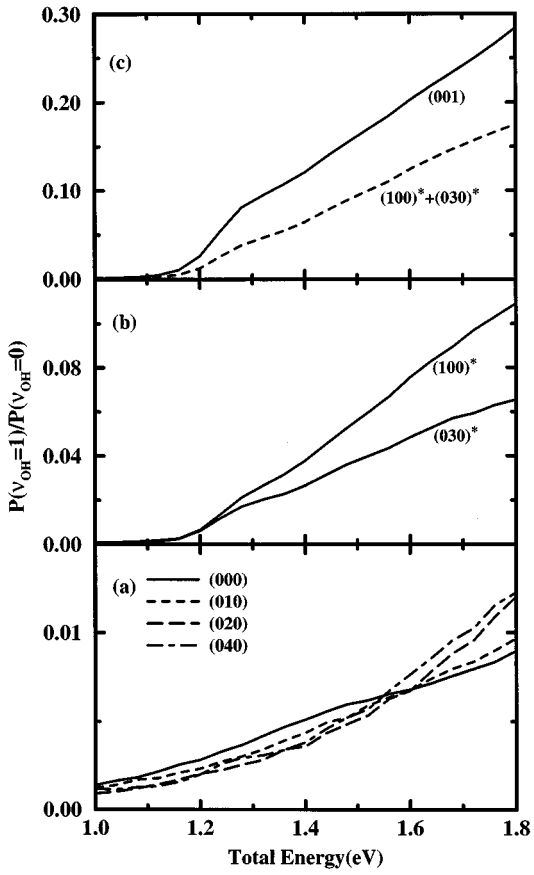

FIG. 7. The product ratio, OH(1)/OH(0), for all states as a function of total energy.

tio, and the quite large ratio for initial (030)* state arises from some substantial component of the symmetric stretching excitation mode in that not pure (030)* state.

Because the probability for produce OH(1) product from the initial bending excited state is very small, the fairly large OH(1) probabilities for the (100)* and (030)* states can only come from the symmetric stretching excited components in these two state. Thus the probabilities to produce OH(1) product from a *pure* initial symmetric stretching excited state roughly equals to the sum of the OH(1) probabilities for (100)* and (030)* states, and the OH(1)/OH(0) for a *pure* initial symmetric stretching excited state would be more or less like the line shown in Fig. 7(c), quite close that for initial (001) state which reaches 28% for total energy equal to 1.8 eV. From Fig. 7(c), we can see that the probabilities to form OH(1) product for initial stretching excited states are much larger than those for initial stretching not excited states. This is because that the product vibrational excitation arises from the OH vibration in the H_2O reactant rather than from excitation during the reaction, as has been discovered by experiments.[49,48,52]

One more interesting point we can find in Fig. 6 is that the P[OH(0)] is essentially saturated at total energy equal to 1.2 eV, and the increase of total reaction probabilities above there almost all comes from P[OH(1)] for initial (001) state.

D. Integral cross sections

The integral cross section for a specific initial state is obtained by summing the reaction probabilities $P^{JM\epsilon}_{\nu_0 L_0 \bar{\Omega}_0}$ over all the partial waves,

$$\sigma_{\nu_0 L_0}(E)=\frac{1}{2L_0+1}\frac{\pi}{k^2}\sum_{J\epsilon\Omega_0}(2J+1)P^{JM\epsilon}_{\nu_0 L_0 \bar{\Omega}_0}(E). \qquad (33)$$

Since the exact close-coupling calculations for $J>0$ state are extremely expensive computationally, the standard CS[59,60] approximation is employed in calculations for $J>0$. The maximum quantum number, $J_{\max}$, needed to converge the cross section, varies from about 15 for the low translational energies to 45 for the highest translational energy. The cross sections are multiplied by a factor of 2 before plotting in Figs. 8 and 9.

Figure 8 shows the integral cross section for H_2O initially in the ground vibration state (000) and the first bending excited state (010) for total energy up to 1.8 eV. As can be seen from the figure, the (000) cross section rises from essentially zero at 0.8 eV and steadily increases with increasing of translational energy, showing a typical threshold behavior. Overall, the cross sections are very small, with $0.37a_0^2$ for 1.8

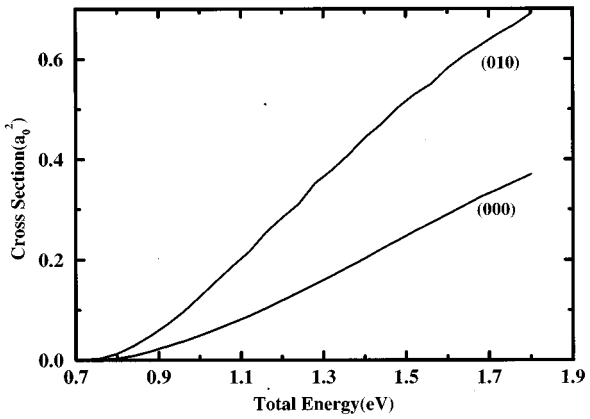

FIG. 8. Integral cross sections for $H+H_2O(\nu_1\nu_2\nu_3)$ reaction as a function of total energy for H_2O initially in (000) and (010) states.

eV, in accord with the small reaction probabilities for the ground rovibrational H_2O shown in Fig. 4. As was found for the total reaction probability for $J=0$, the first bending excitation significantly enhances the cross sections for the reaction. For the *total energy* larger than 0.9 eV the cross section for the (010) state is about twice as large as that for the (000) state. The ratio between the cross sections for (010) and (000) states for lower total energy is even bigger.

The fact that the (010) cross section is significantly larger than the (000) cross section for the same *total energy* indicates that the (010) state will contribute very significantly to the thermal rate constant. For not very high temperature, the contribution will be twice as large as that from the (000) state because the (010) cross section is twice as large as the (000) cross section for *total energy* less than 1.6 eV. From the finding that the (020), (100)*, and (030)* states enhance the reaction probability for the $J=0$ reaction more significantly than the (010) state as shown in Fig. 4, it is very reasonable to expect that these three states will also contribute to the thermal rate constants significantly. So for the WDSE PES, the thermal rate constants for the reaction will mainly come from the first four initial vibrationally excited states, dominating the contribution from the initial ground vibration state to the thermal rate constants. This actually contrasts with what is generally believed by kineticists that excited vibrational states of water are too high in energy to contribute more than a few percent to the rate constant at room temperature.[61] More theoretical and experimental investigations, in particular on the WDSE PES, are necessary to explain the contradiction.

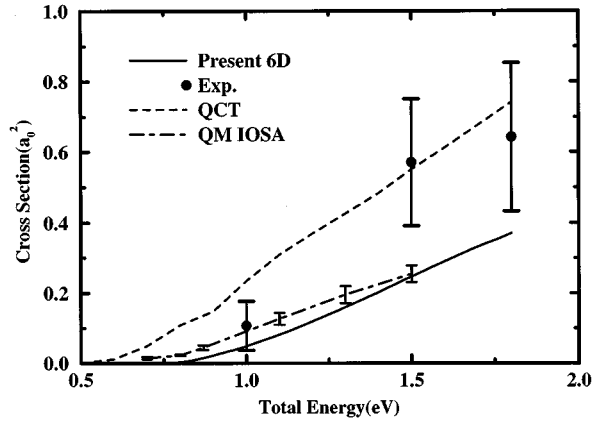

FIG. 9. Comparison of integral cross sections from the present calculation with other theoretical calculations, and with the experimental results. Present results are shown by a solid line, the experiment results Ref. 42 by three solid circles with error bars, QCT results Ref. 29 by a dashed line, and QM IOSA results Ref. 31 by a dot–dashed line.

In Fig. 9, the present cross sections for the initial ground rovibrational H_2O are compared with the results of QCT calculation,[29] the results of recent quantum mechanical IOSA calculation,[31] and the experimental measurements. First, we can see that the QCT cross sections are about twice as large as than the present results in the high energy region, and much larger than the present results in low energy region. The QCT result has a threshold energy about 0.25 eV lower than the present calculation. Since both the QCT and the present calculations were carried out for nonrotating H_2O in the vibrational ground state (000), and the present results should be very accurate for nonrotating $H_2O(000)$ on the given PES despite the employment of CS approximation, it seems obvious that the QCT calculations did not give accurate cross sections for low collision energies. The reason, we believe, is mainly due to the violation of zero point energy conservation in QCT calculations as discussed in Ref. 30. Of course, the accuracy of the CS approximation to this reaction is still waiting to be investigated, although it is generally believed that the CS approximation should be quite good for a reaction with collinear saddle geometry as in the $H+H_2O$ reaction. The cross section from the IOSA calculation is larger than the present results for the total energy less than 1.5eV, and smaller than the present results for higher energies given the trend of the IOSA cross section curve. This result is similar to the comparison between the accurate 6D cross section[19] and IOSA calculation for the reverse reaction, i.e., the $H_2+OH \rightarrow H+H_2O$ reaction.[31] The overall agreement between the present and the IOSA results is better than that between the QCT and the present results, although a large discrepancy also exists in low energy region. Second, we can see that the present cross sections are all smaller than the experimental results by about a factor of 2, and quite close to the lower limits of the error bars for the experimental results. It should be noted that our calculation is for nonrotating H_2O, while the experimental measurements are for the thermal averaging over initial rotations of the reagents. It was found in QCT[27] and 4D quantum[14] calculations that the averaging of initial rotations of H_2O typically populated at room temperature is not important for calculating integral cross sections for the reaction. If this is still true in full dimension quantum calculations, then the discrepancy between the experiment and present calculation can only originate from the WDSE PES used in our calculation.

IV. CONCLUSIONS

A 6D time-dependent wave packet method has been developed to study atom–triatom reactive scattering. The approach employs a new BF coupled total angular momentum basis for three angle coordinates, and three 1D vibrational and translational DVR basis sets for three radial coordinates. By expanding the wave function in such a way, the time-dependent treatment of atom–triatom reactive scattering comes out to be very similar to that for the diatom–diatom reactive scattering.[17–19,23,24] Several techniques developed in time-dependent diatom–diatom reactive scattering study were readily applied to the present study. Although in principle our method is capable of dealing with reactions in which either of the two bonds in a triatomic molecule may be broken, it is more practical to treat one bond in the triatomic molecule as nonreactive for the sake of computational effort. Thus far the present method is able to treat exactly atom–triatom reactions in which there are no identical atoms and only one of the chemical bonds in the triatomic molecule can be broken.

The present method is applied to the simplest atom-triatom reaction $H+H_2O \rightarrow H_2+OH$. Except for the restrictions that all three hydrogen atoms involved in the reaction are distinguishable and only one OH bond in water is able to be broken in the reaction, the calculations are carried out exactly for $J=0$. These restrictions are not likely to have a great effect on the reaction probabilities. The reaction probabilities for ground and vibrationally excited states are reported, along with the final OH vibration distribution. Integral cross sections were also calculated for the ground vibrational state and the first bending excited state by using the CS approximation.

Our calculations show that the total reaction probability is very small for the ground initial vibrational state, and that vibrational excitation of the reactant molecule significantly enhances the reactivity of the system. The excitation energy for the first two bending excited states and two mixed state between the first symmetric stretching and the third bending excited state can all be used to reduce the threshold, while this high efficiency of threshold reduction does not persist for the higher bending overtone, (040) state. The initial symmetric stretching excited state is more efficient in enhancing the reactivity than the initial asymmetric stretching excited state. The product OH is found essentially in the ground vibrational state for reaction from the (000), (010), (020), and (040) states, and it is deduced that the bending excitation has essentially no effect on the final vibrational state of product OH. The probabilities to form OH(1) substantially increase for stretching excited states. The overall qualitative agreement between the present calculations and QCT[27] calculations is quite good in the effect of vibrational excitation of water on the reaction.

The ground vibrational state cross sections are very small due to the small reaction probabilities. The cross section for the reaction from the first bending excited state is essentially twice as large as that from the initial ground vibrational state. We found our calculated cross sections are about half the size of the experimental measurements,[42] and also about half the size of the QCT results[29] in the high energy region. In the low energy region, the difference between the present calculation and the QCT results[29] is even larger, with the QCT threshold about 0.25 eV lower than the present result. We believe this is due to the violation of zero point energy in QCT calculations. The agreement between the present calculations and IOSA calculations[31] for cross section is found to be relatively good.

ACKNOWLEDGMENTS

The research was supported in part by a grant from the Department of Energy, DE-FG02-87ER13679. D. H. Zhang would like to thank Prof. George Schatz for very helpful discussions, and Prof. Joel Bowman, Prof. David Clary, Prof. Micheal Baer, Dr. Desheng Wang, Dr. Henrik Szichman, Dr. Julian Echave for sending the relevant data.

[1] A. N. Brook and D. C. Clary, J. Chem. Phys. **92**, 4178 (1992).
[2] Q. Sun and J. M. Bowman, J. Chem. Phys. **92**, 5201 (1990).
[3] D. C. Clary, J. Chem. Phys. **95**, 7298 (1991).
[4] D. C. Clary, Chem. Phys. Lett. **192**, 34 (1992).
[5] D. C. Clary, J. Chem. Phys. **96**, 3656 (1992).
[6] G. Nyman and D. C. Clary, J. Chem. Phys. **99**, 7774 (1993).
[7] D. Wang and J. M. Bowman, J. Chem. Phys. **96**, 8906 (1992).
[8] D. Wang and J. M. Bowman, Chem. Phys. Lett. **207**, 227 (1993).
[9] J. M. Bowman and D. Wang, J. Chem. Phys. **96**, 7852 (1992).
[10] D. Wang and J. M. Bowman, J. Chem. Phys. **98**, 6235 (1993).
[11] H. Szichman, I. Last, A. Baram, and M. Baer, J. Phys. Chem. **98**, 828 (1994).
[12] H. Szichman and M. Baer, J. Chem. Phys. **101**, 8620 (1994).
[13] D. C. Clary and G. C. Schatz, J. Chem. Phys. **99**, 4578 (1993).
[14] J. Echave and D. C. Clary, J. Chem. Phys. **100**, 402 (1994).
[15] W. H. Thompson and W. H. Miller, J. Chem. Phys. **101**, 8620 (1994).
[16] E. M. Goldfield, S. K. Gray, and G. C. Schatz, J. Chem. Phys. **102**, 8807 (1995).
[17] D. H. Zhang and J. Z. H. Zhang, J. Chem. Phys. **99**, 5615 (1993).
[18] D. H. Zhang and J. Z. H. Zhang, J. Chem. Phys. **100**, 2697 (1994).
[19] D. H. Zhang and J. Z. H. Zhang, J. Chem. Phys. **101**, 1146 (1994).
[20] U. Manthe, T. Seideman, and W. H. Miller, J. Chem. Phys. **99**, 10078 (1993).
[21] U. Manthe, T. Seideman, and W. H. Miller, J. Chem. Phys. **101**, 4759 (1994).
[22] D. Neuhauser, J. Chem. Phys. **100**, 9272 (1994).
[23] D. H. Zhang and J. Z. H. Zhang, Chem. Phys. Lett. **232**, 370 (1995).
[24] D. H. Zhang *et al.*, J. Chem. Phys. **102**, 7400 (1995).
[25] D. H. Zhang and J. Z. H. Zhang, J. Chem. Phys. **103**, 6512 (1995).
[26] H. Elgersma and G. C. Schatz, Int. J. Quantum Chem. Symp. **15**, 611 (1981).
[27] G. C. Schatz, M. C. Colton, and J. L. Grant, J. Phys. Chem. **88**, 2971 (1984).
[28] K. Kudla and G. C. Schatz, Chem. Phys. Lett. **193**, 507 (1992).
[29] K. Kudla and G. C. Schatz, J. Chem. Phys. **98**, 4644 (1993).
[30] K. Kudla and G. C. Schatz, Chem. Phys. **175**, 71 (1993).
[31] H. Szichman and M. Baer, Chem. Phys. Lett. **242**, 285 (1995).
[32] S. P. Walch and J. T. H. Dunning, J. Chem. Phys. **72**, 1303 (1980).
[33] G. C. Schatz and H. Elgersma, Chem. Phys. Lett. **73**, 21 (1980).
[34] G. C. Schatz, J. Chem. Phys. **74**, 1133 (1981).
[35] C. P. Fenimore and G. W. Jones, J. Phys. Chem. **62**, 693 (1958).
[36] G. Dixon-Lewis, M. M. Sutton, and A. Williams, Trans. Faraday Soc. **61**, 255 (1965).
[37] S. Madronich and W. Felder, J. Phys. Chem. **88**, 1857 (1984).
[38] J. V. Michael and J. W. Sutherland, J. Phys. Chem. **92**, 3853 (1988).
[39] K. Kleinermanns and J. Wolfrum, Appl. Phys. B **34**, 5 (1984).
[40] A. Jacobs, H. R. Volpp, and J. Wolfrum, *24th International Symposium on Combustion* (The Combustion Institute, Pittsburgh, PA, 1992).

[41] A. Jacobs, H. R. Volpp, and J. Wolfrum, Chem. Phys. Lett. **196**, 249 (1992).
[42] A. Jacobs, H. R. Volpp, and J. Wolfrum, J. Chem. Phys. **100**, 1936 (1994).
[43] K. Kessler and K. Kleinermanns, Chem. Phys. Lett. **190**, 145 (1992).
[44] K. Honda, M. Takayanagi, T. Nishiya, H. Ohoyama, and I. Hanazaki, Chem. Phys. Lett. **180**, 321 (1991).
[45] A. Sinha, M. C. Hsiao, and F. F. Crim, J. Chem. Phys. **92**, 6333 (1990).
[46] A. Sinha, J. Phys. Chem. **94**, 4391 (1990).
[47] F. F. Crim, M. C. Hsiao, J. L. Scott, A. Sinha, and R. L. van der Wal, Philos. Trans. R. Soc. London Ser. A **332**, 259 (1990).
[48] A. Sinha, M. C. Hsiao, and F. F. Crim, J. Chem. Phys. **94**, 4928 (1991).
[49] M. C. Hsiao, A. Sinha, and F. F. Crim, J. Phys. Chem. **95**, 8263 (1991).
[50] F. F. Crim, A. Sinha, M. C. Hsiao, and J. D. Thoemke, *Mode Selective Chemistry*, edited by J. Jortner, R. D. Levine, B. Pullman (Kluwer, Dordrecht, 1991).
[51] M. J. Bronikowski, W. R. Simpson, B. Girad, and R. N. Zare, J. Chem. Phys. **95**, 8647 (1991).
[52] M. J. Bronikowski, W. R. Simpson, B. Girad, and R. N. Zare, J. Phys. Chem. **97**, 2194 (1993).
[53] M. J. Bronikowski, W. R. Simpson, B. Girad, and R. N. Zare, J. Phys. Chem. **97**, 2204 (1993).
[54] J. Z. H. Zhang *et al.*, J. Chem. Phys. **88**, 2492 (1988).
[55] J. M. Launay, J. Phys. B **10**, 3665 (1977).
[56] J. Z. H. Zhang, J. Chem. Phys. **94**, 6047 (1991).
[57] J. A. Fleck, Jr, J. R. Morris, and M. D. Feit, Appl. Phys **10**, 129 (1976).
[58] G. C. Schatz and S. P. Walch, J. Chem. Phys. **72**, 776 (1980).
[59] R. T. Pack, J. Chem. Phys. **60**, 633 (1974).
[60] P. McGuire and D. J. Kouri, J. Chem. Phys. **60**, 2488 (1974).
[61] G. C. Schatz (private communication).